Surface morphology of Kr⁺-polished amorphous Si layers

A. J. R. van den Boogaard,[a] E. Louis, and E. Zoethout
FOM Institute for Plasma Physics Rijnhuizen, P.O. Box 1207, NL-3430BE, Nieuwegein, The Netherlands

S. Müllender
Carl Zeiss SMT AG, D-73466 Oberkochen, Germany

F. Bijkerk
FOM Institute for Plasma Physics Rijnhuizen, P.O. Box 1207, NL-3430BE, Nieuwegein, The Netherlands
and MESA Institute for Nanotechnology, University of Twente, P.O. Box 217, NL-7500AE Enschede,
The Netherlands

The surface morphology of low-energy Kr⁺-polished amorphous Si layers is studied by topographical methods as a function of initial substrate roughness. An analysis in terms of power spectral densities reveals that for spatial frequencies $2 \times 10^{-2} - 2 \times 10^{-3}$ nm⁻¹, the layers that are deposited and subsequently ion polished reduce the initial substrate roughness to a rms value of 0.1 nm at the surface. In this system, the observed dominant term in linear surface relaxation, proportional to the spatial frequency, is likely to be caused by the combined processes of (a) ion-induced viscous flow and (b) annihilation of (subsurface) free volume during the ion-polishing treatment. Correspondingly, a modification of the generally assumed boundary conditions, which imply strict surface confinement of the ion-induced viscous flow mechanism, is proposed. Data on surface morphology are in agreement with the optical response in extreme ultraviolet from a full Mo/Si multilayered system deposited onto the modified substrates. © *2010 American Vacuum Society.* [DOI: 10.1116/1.3428545]

I. INTRODUCTION

Many applications of thin-film systems critically depend on the smoothness of surfaces and interfaces. In this perspective, epitaxial (multi)layers can meet the highest quality demands but generally require strictly defined deposition conditions. Ultrasmooth amorphous layers of nanometer thickness are more routinely realizable and typically have rms roughness values in the order of 0.1 nm. Studies of the corresponding thin-film growth kinetics require surface morphological characterization of these layers. In the absence of large surface slopes, the theoretical framework of a linear continuum model can be applied to amorphous thin-layer surface morphology evolution down to the nanometer scale, involving a layer-intrinsic and a substrate-replicated component.[1,2]

As a function of layer thickness (t), the surface morphology in the spatial frequency (f) domain in terms of two-dimensional power spectral densities (PSDs) is given by[3]

$$\text{PSD2}D(q,t) = \frac{4\Omega}{2\pi} \frac{1 - e^{-2b(q)t}}{b(q)} + e^{-2b(q)t}\text{PSD2}D(q)$$

$$\equiv \Gamma_t[\text{PSD2}D(q)] \tag{1}$$

with

$$b(q) = \sum_i \nu_i q^i. \tag{2}$$

Here $q = 2\pi f$ and Ω is the volume of a unit cell. For $b \to 0$,

the Poisson-like distribution of unit cells over a surface, due to the random nature of layer growth or removal in the absence of redistributing processes, is referred to as stochastical roughness. The polynomial $b(q)$ gives a measure of the kinetic processes proportional to q to the power i, with corresponding proportionality constants ν_i.

For the angular window 35°–60° from the surface normal, smooth Si surfaces have been shown to be stable under noble gas ion sputtering without strong dependence on ion species or energy.[4] A further study of the stabilizing kinetics may be of relevance to obtain a more general description of surface morphology in terms of ion-beam parameters, including sharp transitions between stable and unstable regimes.[5] In this study, we focus on a thin-layer a-Si physical vapor deposition (PVD) at room temperature, modified by low-energy Kr⁺ ions impinging on the surface at an angle of 50° to the surface normal. These conditions enable ion polishing of the Si layers and deposition of Mo/Si extreme ultraviolet (EUV) reflective multilayer systems with high quality interfaces.[6–9]

Due to the low thermal energy of the evaporant (<1 eV) compared to binding energies, stochastical roughening typically dominates the PVD thin-layer morphology. The combined effect of layer growth and subsequent ion-induced sputtering and surface relaxation follows from iterative application of Eq. (1), with indices d and p relating to the deposition ($b \to 0$) and ion polishing ($b(q) > 0$), respec-
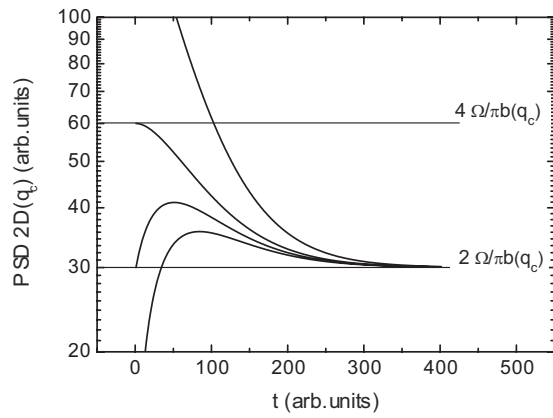
[a]Electronic mail: a.j.r.vandenboogaard@rijnhuizen.nl

FIG. 1. Calculated PSDs at given spatial frequency q_c and $\Omega=0.6$ for different initial values [PSD2$D(q_c,t=0)=$10, 30, 60, and 200], plotted as a function of deposited [$b(q_c)\to0$] and removed [$b(q_c)=0.05$] layer thicknesses t (all arb. units).

tively: PSD2$D(q,t)=\Gamma_t^p\Gamma_t^d[$PSD2$D(q)]$. At a given spatial frequency q_c, the expression will eventually reach an asymptotic value of $2\Omega/\pi b(q_c)$ with increasing thickness, independent of the initial value ($t=0$), of which an example is given in Fig. 1. For an initial value PSD2$D(q_c,t=0)$ $=4\Omega/\pi b(q_c)$, a monotonic decrease toward the asymptote is observed. The corresponding morphology changes are thus preferably studied on a model system with slightly elevated initial roughness levels, since the expected modifications are unambiguous and more pronounced than on surfaces with initial roughness close to the asymptote (rms roughness≈0.1 nm). We used substrates with a rms roughness up to 0.7 nm to obtain an insight into the kinetics corresponding to low-energy Kr+ polishing of PVD *a*-Si. The possibilities of reducing initial substrate roughness by increasing deposited and sputtered layer thicknesses have been studied. The results are examined in terms of PSDs obtained by atomic-force microscopy (AFM) and optical profiler and in terms of EUV reflectance after depositing Mo/Si multilayers on the modified substrate morphologies.

II. EXPERIMENT

A. Substrates and roughness characterization

The substrates used to study the thin-layer roughness evolution are samples made from (superpolished) fused-silica and ultralow thermal expansion quartz (ULE). A range in the ULE substrate roughness was obtained by aborting the superpolishing process at different stages. At three positions on each sample, the two-dimensional surface-height profiles were measured by AFM and optical profiler pre- and post-deposition. The areas probed were 1×1 and 10×10 μm^2 for AFM and 245×245 μm^2 for the optical profiler with noise values of 0.03, 0.05, and 0.07 nm in rms roughness, respectively. By AFM, the spatial frequencies $10^{-1}-3\times10^{-4}$ nm^{-1} were probed, while the optical profiler provided information on lower spatial frequencies, namely, $3\times10^{-4}-10^{-5}$ nm^{-1}. The substrate rms roughness varied from

approximately 0.1 nm for the fused-silica substrates to 0.2–0.7 nm for the ULE substrates, as calculated by integrating over the entire spatial frequency range.

B. Deposition procedure

Experiments were performed at room temperature under high-vacuum conditions with a base pressure of 10^{-8} mbar.[10] The PVD was performed from an e-beam generated vapor of the target material onto the substrates mounted in the vacuum vessel. Thickness control was provided by *in situ* quartz-crystal mass balances and soft x-ray reflectometry on a superpolished Si monitor wafer mounted in the center of the substrate holder. A Kaufmann source was used to generate the Kr+ beam. Continuous sample rotation (60 rpm) was applied to enhance layer thickness uniformity and to suppress possible ion-induced ripple formation.[11]

The deposition scheme of each experiment incorporated an initial layer of Mo of 2 nm thickness to enable grounding of the nonconductive substrates and inhibit charge building up during ion polishing. Subsequently, a Si layer of approximately 20 nm was deposited and removed afterwards by ion sputtering during the Kr+ polishing at 50° normal angle. The Si deposition and polishing cycle were performed repetitively, where during the first cycle a 4–10 nm (depending on ion energy) excess Si layer served as a spacer layer to prevent Kr+ interaction with the buried Mo/Si interface. The obtained thin-film system is referred to as a Si single layer, in contrast to the Mo/Si multilayers optimized for the EUV reflection, which are additively deposited on the Si single layers in a later stage.

The Kr+ polishing was employed at 130 eV and 2 keV. Minimized ion-induced intermixing of subsurface interfaces, e.g., in multilayer systems, can be obtained at the lower energy regime,[12] while at 2 keV the ion treatment has an extended in-depth range at a given fluence due to the higher sputter yield. The Si single layer deposition/polishing cycles were performed 1, 5, and 18 times at 130 eV and 18 and 46 times at 2 keV during individual experiments. The maximum number of cycles at both energies was limited by experimental time. Typical removal rates were $R=10^{-2}$ nm/s and $R=7\times10^{-2}$ nm/s for 130 eV and 2 keV ion polishing, respectively.

C. EUV specular reflectometry

After characterization of the surface morphology of the Si single layers, a 50-period Mo/Si multilayer optimized for EUV reflectance was deposited on the samples. Per period 0.5 nm as-deposited Si was removed by 130 eV Kr+ polishing. The effect of the surface morphologies of the various Si single layers, thus acting as substrates for high reflectance multilayers, is examined by reflectance characterization. For comparison, Mo/Si multilayers were codeposited on substrates with varying roughness without application of Si single layers. Near-normal (1.5° angle of incidence) specular EUV reflectance was measured by the Physikalisch-Technische Bundesanstalt at the electron-storage ring BESSY II in Berlin.[13]
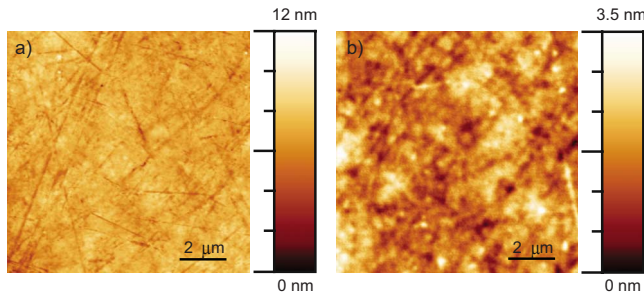
FIG. 2. (Color online) Substrate and 18-cycle 130 eV Si single layer AFM topographies: (a) predeposition, rms=0.51 nm and (b) postdeposition, rms =0.17 nm.

III. RESULTS AND DISCUSSION

A. PSD analysis

From the topographical height profiles obtained by AFM and optical profiler (Fig. 2), combined PSDs on the spatial frequency range $10^{-1}-10^{-5}$ nm^{-1} were extracted. For the ULE substrates, the typical shape of the PSD curves suggests a division in three spatial frequency domains [Fig. 3(a)]. At the very high spatial frequencies (i), $10^{-1}-2\times10^{-2}$ nm^{-1}, the PSDs pre- and postdepositions show differences in the order of the noise level of the AFM measurements. At spatial frequencies (ii), $2\times10^{-2}-1\times10^{-3}$ nm^{-1}, the substrate roughness is significantly reduced. This domain tends to expand toward lower spatial frequencies with the number of Si single layer cycles, but the dependency is only moderate. At spatial frequencies (iii), $<1\times10^{-3}$ nm^{-1}, no significant differences in PSDs pre- and postdepositions are observed and the substrate morphology is fully replicated.

An overview of the roughness mitigation is obtained by calculating the rms roughness values for spatial frequencies $2\times10^{-2}-2\times10^{-3}$ nm^{-1} [Fig. 3(b)]. The low correlation in rms roughness pre- and postdepositions indicates a restricted memory of substrate morphology for 18 Si single layer cycles or more, where the rms roughness approaches a lower limit of $0.1-0.14\pm0.02$ nm postdeposition, depending on the initial substrate roughness. No ion energy dependence is observed, indicating that the layer surface morphology is mainly determined by the number of cycles, hence the total deposited and removed layer thickness.
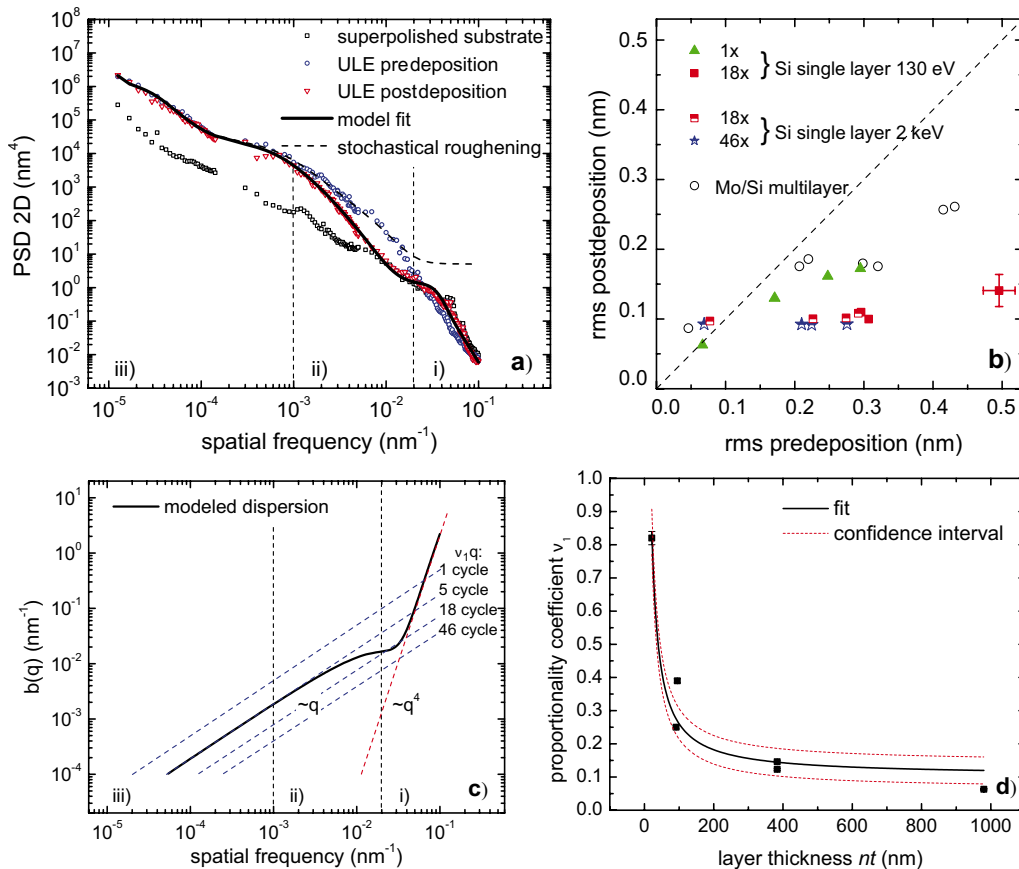

FIG. 3. (Color online) (a) Example of PSDs of a superpolished fused-silica substrate, and of a ULE substrate pre- and post-5-cycle 130 eV Si single layer deposition. A model fit to the data is shown, as well as the calculated layer PSD due to stochastical growth and removal only. (b) Postdeposition rms surface roughness as a function of initial substrate roughness (predeposition). Data averaged over three measuring points per sample, for spatial frequencies $2\times10^{-2}-2\times10^{-3}$ nm^{-1}. Data with rms roughness predeposition <0.1 nm correspond to superpolished fused-silica samples. (c) Typical dispersion relation (2), as obtained by the model fit to the measured PSDs (a). The corresponding asymptote $\sim q^4$ is depicted, as well as $\sim q$ for the different Si single layers. (d) Proportionality coefficient ν_1 as a function of total layer thickness. The solid line represents a fit of Eq. (3) to the data for $\Delta t=20$ nm, $V=0.1\pm0.04$, and $V_0=0.89\pm0.07$. Confidence interval based on 1 standard error in V and V_0 is shown.

A more general explanation of the data is obtained by fitting the linear model to the PSDs. Model equation (1) is iteratively applied to the PSD of the substrate surface up to the total number of cycles n, denoted by the subscript: $PSD2D(q,t)_n = \Gamma_t^p \Gamma_{t\,(n)}^d \Gamma_t^p \Gamma_{t\,(n-1)}^d \cdots \Gamma_t^p \Gamma_{t\,(1)}^d [PSD2D(q)]$.

The number of fitting parameters is limited by choosing the unit cell Ω during both deposition and ion polishing equal to the average volume of a Si atom in amorphous Si, yielding 0.02 nm^3 at a density of 2.2 g/cm^3. During deposition, no kinetic processes are considered to be present and the corresponding parameters are used in the limit $b \xrightarrow{lim} 0$, while for ion polishing the proportionality coefficients in Eq. (2) are used as free-fitting parameters. The data for the superpolished fused-silica substrates are excluded from the fitting due to the low roughness values compared to experimental noise.

It is found that the linear model provides an accurate description of the data, of which an example is shown in Fig. 3(a). During ion polishing, Eq. (2) is dominated by a term $\propto q$ for spatial frequencies $< 10^{-2}$ nm^{-1} and by a term $\propto q^4$ for spatial frequencies $> 3 \times 10^{-2}$ nm^{-1}. In between, a negative proportionality in q^2 yields a minimum indicating less, but still positive, smoothing. A typical full dispersion function given by the first, second, and fourth orders in q and corresponding coefficients ν_1, ν_2, and ν_4 is shown in Fig. 3(c), emphasizing the importance of the linearity in q at domain (ii).[12,14] At the spatial frequency domain (i), a relatively large contribution of stochastical roughness counterbalances the smoothing kinetics [Fig. 3(a)]. For the lower spatial frequencies at domain (iii), the effective replication of the PSD of the substrate relates to the decrease in dispersion over orders of magnitude.

The fitting parameters ν_i show a dropoff with the number of Si single layer cycles. This observation is particularly significant for ν_1 [Fig. 3(d)], being mainly determined by data of high signal-to-noise ratio at spatial frequencies where the higher-order terms in kinetics are negligible [domains (ii) and (iii), Figs. 3(a) and 3(c)]. The decay is reciprocally proportional to the total removed layer thickness, which indicates that, as now will be derived, ν_1 may give an effective measure of multiple linear stages in kinetics behaving $\propto q$. Since stochastical roughening is small as compared to substrate PSD at domains (ii) and (iii) [Fig. 3(a)], the left term on the right-hand side of Eq. (1) can be neglected, explicitly listing the dependence on ν_1: $PSD2D(q,t,\nu_1)_n = e^{-2\nu_1 nt} PSD2D(q)$ with nt being the total removed layer thickness. Now consider the kinetics to have an initially elevated value (V_0), e.g., during the first cycle, and a value (V) during all later stages; $\nu_1 \rightarrow V_0$ for $t \leq \Delta t$ and $\nu_1 \rightarrow V$ for $\Delta t < t \leq nt$, yielding the exponent in the latter PSD expression to become $-2(V(nt - \Delta t) + V_0 \Delta t)$. When bound to a single model parameter ν_1^*, it will transform under the stated substitution to the weighted mean over the stages in surface-relaxing kinetics, as in this example,

$$\nu_1^*(nt, \Delta t, V_0, V) = \frac{V(nt - \Delta t) + V_0 \Delta t}{nt}. \qquad (3)$$

The main trend in the data is explained by Eq. (3). It follows that $V_0 > V$, although the values of V_0 and V cannot be determined uniquely without *a priori* assuming a layer thickness of Δt. In consequence the initially elevated rate in smoothing kinetics cannot further be quantified at this point but its occurrence may be related to a structural or chemical nonequilibrium of the deposited Si single layer prior to completion of the first Si single layer cycle and primary treatment of the subsurface Mo/Si interface region with Kr+ ions.

1. Kinetics

The dispersion relation $b(q)$ as obtained by the model fitting procedure reveals the fundamentals of the ion-induced surface modification. The proportionality with $-q^2$ is generally interpreted as a fingerprint of roughening due to the local surface curvature-dependent sputter yield variations.[15] The q^4 dependency may either represent surface diffusion[16,17] or surface-layer-confined viscous flow.[18] The latter effect is argued to be dominant for ion-damaged disordered surfaces[19,20] similar to the surfaces under consideration. The constraint of surface-confined viscosity implies the boundary condition of no slip at the viscous liquid-solid interface and relates to the restricted penetration depth of the ions. The term linear in q in the dispersion is traditionally explained as due to bulk viscous flow[16,17] having an in-depth extension into the system $> 1/q$ nm.[18] Although occurrence of this process is physically inexplicable for the system under consideration due to the superficial character of the ion-polishing treatment, the observed dispersion gives a robust indication of surface relaxation caused by mass transport extending the strict surface confinement of the ion-induced viscous layer. A revision of the mentioned model boundary condition is proposed to resolve this discrepancy.

2. Free volume annihilation

Analysis of the critical angle in hard x-ray reflectance shows an increased density of e-beam PVD Si layers grown during simultaneous 130 eV Kr+-assistance as compared to the as-deposited layers (Fig. 4). This effect is partly due to the incorporation of typically 1 at. % Kr into the a-Si, but based on each Kr atom replacing a Si atom in the amorphous matrix still 2.5% of the densification can be addressed to a decreased fraction of in-layer free volume. It is expected that the ion-polishing treatment as applied to the as deposited, relatively porous Si layers will give rise to a similar compaction, associated with ion-induced in-depth mass transport over short length scales. The mass transport as facilitated by the gradient in free volume from the dense ion-induced viscous layer to the underlying as-deposited material is referred to as free volume annihilation (FVA). Although the process of FVA opposes the gradient in free volume, it is maintained during ion polishing due to simultaneous sputtering and thus continuous renewing of the surface layer.
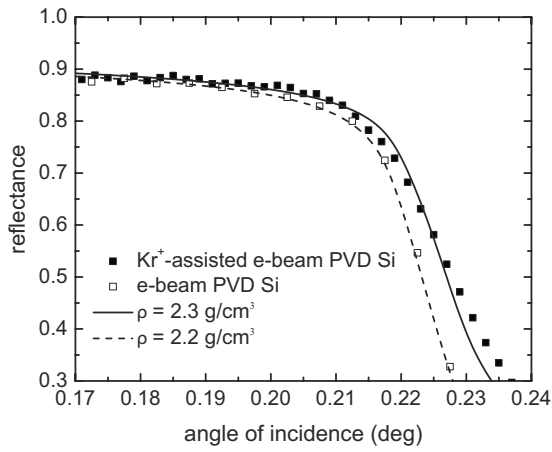
FIG. 4. Reflectance of 0.154 nm Cu $K\alpha$ radiation from Si layers as a function of grazing angle of incidence. Measured data and simulations for two layer densities are shown.

FIG. 6. Calculated dispersion relation for parameter values given in Table I.

Allowing for FVA requires small adjustments in the boundary conditions proposed by Orchard[18] and will be demonstrated to resolve the discrepancy as stated in Sec. III A 1. The restriction of no slip at the interface between the a-Si and the ion-induced viscous layer [Fig. 5(a)] is mitigated for in-depth mass transport in the y direction [Fig. 5(b)], with x and y the perpendicular axes of a Cartesian coordinate system. With x as the only variable, the velocity at the interface $(x,-h)$ can be written as $\vec{v}(x,-h)=(s_x,s_y)(-h)+(\omega_x,\omega_y)(x,-h)$, in which the constant velocity component is attributed to uniform compacting mechanisms like ion-atom forward scattering events, and the lateral position depending velocity
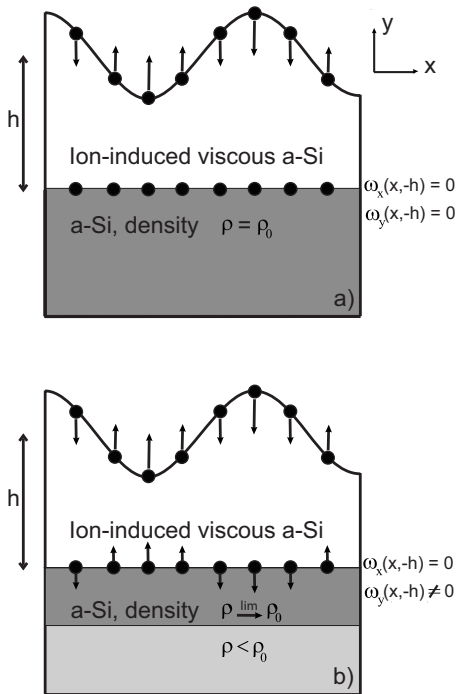

FIG. 5. Schematic representation of surface-confined viscous flow (a) for the condition of no slip at the liquid-solid interface at $(x,-h)$, (b) allowing for mass transport in the y direction through the interface.
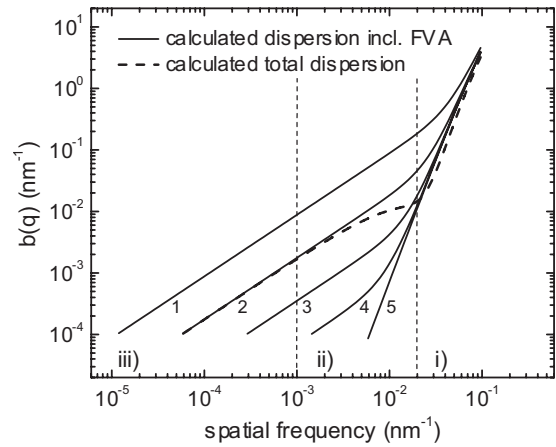
component to stress opposing the free surface perturbations from equilibrium. In the absence of a rigid interface, the latter velocity component is assumed proportional to the velocity in an infinitely thick layer of sinusoidal perturbed viscous fluid in the y direction:[17] $\omega_y(x,-h)\propto-iqe^{iqx-qh}(qh+1)=-iqe^{iqx}+O(q^3)$. When ignoring the uniform compaction, this results in the following boundary conditions at the $(x,-h)$ plane in close approximation (second order in q):

$$\omega_x(x,-h)=0,$$

$$\omega_y(x,-h)=-i\frac{\gamma a}{2\eta}q\mu e^{iqx}. \qquad (4)$$

Here γ is the surface tension, a is the amplitude of a Fourier component, η is the viscosity of the surface layer, and $0\leq\mu\leq1$ is a material and structural intrinsic proportionality constant, accounting for the influence of additional friction on the flow velocity ω_y, as compared to the case of an infinitely thick layer of viscous material ($\mu=1$). From Eq. (4), the rate of leveling of surface roughness can be calculated straightforwardly, in analogy with the method described.[18]

Figure 6 shows the calculated dispersion for different values of μ (Table I). The ion-induced viscous surface layer is taken to be 1 nm thick, $h=1$ nm, in which the majority of the primary ion-atom collision events take place.[21] For the limiting values $\mu=0$ and $\mu=1$, the dispersions appear to result from surface-confined viscous flow ($\propto q^4$) and bulk viscous flow ($\propto q$), respectively. For values of μ in between these extrema, a transition from $\propto q$ to $\propto q^4$ for increasing

TABLE I. Parameter values corresponding to dispersion curves Fig. 6.

Dispersion curve No., Fig. 6	$\gamma/(\eta R)$ [a]	μ
1	1.4×10^2	1×10^{-2}
2	1.4×10^2	2×10^{-3}
3	1.4×10^2	4×10^{-4}
4	1.4×10^2	8×10^{-5}
5	1.4×10^2	$<10^{-5}$

[a]R=removal rate.

spatial frequency unifies the two terms. When adding the (negative) proportionality constant ν_2 to take into account surface roughening resulting from local surface curvature-dependent sputter yield variations,[15] full agreement of the modeled dispersion with experiment is obtained. For literature value[22] $\gamma = 0.7$ N m^{-1}, the found viscosities are $\eta = 7 \times 10^7$ and $\eta = 5 \times 10^8$ Pa s for $R = 7 \times 10^{-2}$ nm/s (2 keV Kr⁺) and $R = 10^{-2}$ nm/s (130 eV Kr⁺), respectively. Making use of typical sputter yields of Si (Refs. 23 and 24) (0.1 and 1 atom/ion, for 130 eV and 2 keV Kr⁺, respectively), and the estimated number of ion-induced displacements per atom (dpa) in the ion treaded layer-volume[21] (2.5 and 20 vacancies/ion, for 130 eV and 2 keV Kr⁺, respectively), the viscosities can be expressed as $\eta = 1 \times 10^8$ Pa dpa, for both ion energies. This value is of the same order as obtained from the classical molecular dynamics simulations on 1 keV self-sputtering of a-Si.[20] The relation between μ and the internal structure of the Si layers is not revealed by the performed experiments but due to lower friction, μ is expected to increase with porosity of the Si layer, resulting in a further enhanced ion-induced modification of the surface morphology in the regime where the dispersion is proportional to q. In this light, the enhanced smoothing kinetics during the first Si single layer cycle could be due to a lower density of the Si layer near the Mo/Si interface region.

B. EUV reflectance analysis

Interface roughness in EUV-reflecting Mo/Si multilayers, partly replicated from the substrate, will induce diffuse scatter at the expense of specular EUV reflectance for spatial frequencies down to a lower limit f_{scat}, given by the expression[25] $m\lambda f_{scat} = |\sin(\alpha \pm \Delta\alpha) - \sin\alpha|$. Here α is the normal angle of incidence and specular reflection, $\Delta\alpha$ is the angular acceptance of the reflectometer detector from the specular beam, λ is the wavelength of the radiation, and m is the order of diffraction. Substrate morphology can thus be related to specular EUV reflectance and vice versa. Si single layer modified substrates of varying roughness were applied with a Mo/Si multilayer for reflectance analysis, with $f_{scat} = 6.7 \times 10^{-4}$ nm^{-1} for the used reflectometer.[13] Scattered light from lower spatial frequency roughness will contribute to the measured signal.

EUV peak reflectance values are plotted as a function of the rms substrate roughness on the relevant spectral roughness interval [Fig. 7(a)]. To compensate for run-to-run reproducibility errors in multilayer periodicity, reflectance values are normalized to the reflectance of the superpolished *in situ* monitoring sample having a roughness of approximately 0.1 nm. It is found that the decrease in substrate roughness by applying the Si single layers significantly enhances the EUV reflectance, although losses compared to untreated superpolished fused-silica substrates are still observed. On the ULE substrates with rms roughness between 0.2 and 0.4 nm, application of the 46-cycle Si single layer results in a 3% higher peak reflectance (only marginally higher than obtained by application of the 18-cycle Si single layer), while at a roughness of 0.7 nm, up to 8% reflectance is gained by
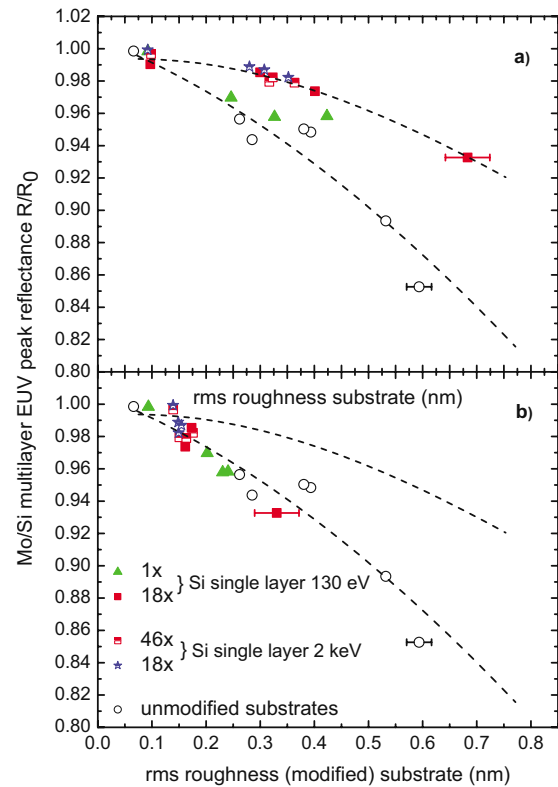

FIG. 7. (Color online) Normalized EUV reflectance from Mo/Si multilayers, with and without underlying Si single layer, on substrates with varying roughness at spatial frequencies $6.7 \times 10^{-4} - 10^{-1}$ nm^{-1}. Fits through ($\bigcirc$) and ($\blacksquare$) serve to guide the eye. (a) Reflectance plotted against initial substrate roughness. (b) Reflectance plotted against starting roughness prior to Mo/Si multilayer deposition (substrate- or Si single layer surface roughness).

applying the 18-cycle 130 eV Si single layer. The independence of surface morphology modification on ion energy, as observed by the AFM measurements, is confirmed by the similarity in EUV reflectance at the 18-cycle Si single layer modified substrates.

Figure 7(b) shows a similar reflectance analysis, but in terms of rms roughness of the surface upon which the multilayer is deposited: the substrate (for the reference samples) or the Si single layer surface. It follows that reflectance of multilayers on the Si single layer modified substrates coincides with the reference data (open circles), despite significant modification of surface morphology and corresponding differences in the shape of the PSD curves, revealing a critical dependence on rms roughness. Due to the similar roughness of the superpolished substrates and the most effectively smoothened ULE substrates (18- and 46-cycle Si single layers) at spatial frequency domains (i) and (ii), the remaining reflectance differences are explained by a still higher roughness at spatial frequencies $2 \times 10^{-3} - 6.7 \times 10^{-4}$ nm^{-1} at which substrate roughness is efficiently replicated by the Si single layers.

IV. CONCLUSIONS

A surface roughness analysis in terms of PSDs obtained from topographies determined by AFM and optical profiler

has revealed the possibility to apply e-beam PVD of Si and subsequent low-energy Kr+ polishing to produce thin layers with a surface roughness which is significantly reduced as compared to the initial substrate roughness. We have applied an increasing number of Si single layer deposition and polish cycles (up to 46), at each of which 20 nm of Si is deposited and removed by Kr+ polishing. Integrated over the spatial frequency range $2 \times 10^{-3} - 2 \times 10^{-2}$ nm^{-1}, substrate roughness values were reduced by a factor 3 toward a value of $0.1 - 0.14 \pm 0.02$ nm. The surface morphology modification shows a critical dependence on the number of cycles, hence the total amount of deposited and removed material, rather than on ion energy. The linear model of roughness evolution is found to be in close agreement with the data and was applied to gain an insight into the fundamentals of the surface relaxation kinetics. The thus-obtained dispersion in kinetics typically shows linearity in spatial frequency. This relation cannot be explained in terms of known mechanisms, such as surface-confined viscous flow, where the viscous relaxation would take place in a strictly confined thin surface layer. The here-suggested modification of the corresponding model boundary conditions allows for in-depth mass transport into the ion polished layer and agrees with the dispersion as observed. This mass transport is argued to be related to ion-induced annihilation of free volume in the Si layer which has, as deposited, a relatively low density compared to the bulk material.

Applying these layer growth and ion-polishing conditions on rough substrates prior to the deposition of a full Mo/Si multilayer reflective Bragg system enhances the EUV reflectance by up to 8%, which is in qualitative agreement with the observed ion-induced substrate smoothing. In particular, the rms roughness at the relevant spatial frequencies is demonstrated to be a good indication of the EUV reflectance of such multilayer systems. The linear model of roughness evolution provides a theoretical framework suited for exploration of further potential enhancement of the ion-modified layer growth characteristics of smooth PVD Si films for applications such as, but not restricted to, EUV optics.

[1] W. M. Tong and R. S. Williams, Annu. Rev. Phys. Chem. **45**, 401 (1994).
[2] D. G. Stearns, Appl. Phys. Lett. **62**, 1745 (1993).
[3] R. Schlatmann, J. D. Shindler, and J. Verhoeven, Phys. Rev. B **54**, 10880 (1996).
[4] F. Frost, B. Ziberi, A. Schindler, and B. Rauschenbach, Appl. Phys. A: Mater. Sci. Process. **91**, 551 (2008).
[5] C. S. Madi, B. Davidovitch, H. B. George, S. A. Norris, M. P. Brenner, and M. J. Aziz, Phys. Rev. Lett. **101**, 246102 (2008).
[6] E. J. Puik, M. J. van der Wiel, H. J. Zeijlemaker, and J. Verhoeven, Rev. Sci. Instrum. **63**, 1415 (1992).
[7] E. Louis *et al.*, Microelectron. Eng. **23**, 215 (1994).
[8] I. Nedelcu, R. W. E. van de Kruijs, A. E. Yakshin, F. Tichelaar, E. Zoethout, E. Louis, H. Enkisch, S. Muellender, and F. Bijkerk, Thin Solid Films **515**, 434 (2006).
[9] A. E. Yakshin, E. Louis, P. C. Görts, E. L. G. Maas, and F. Bijkerk, Physica B **283**, 143 (2000).
[10] E. Louis *et al.*, Microelectron. Eng. **21**, 67 (1993).
[11] R. M. Bradley, Phys. Rev. E **54**, 6149 (1996).
[12] H.-J. Voorma, E. Louis, F. Bijkerk, and S. Abdali, J. Appl. Phys. **82**, 1876 (1997).
[13] C. Laubis *et al.*, Proc. SPIE **6151**, 61510I (2006).
[14] D. G. Stearns, P. B. Mirkarimi, and E. Spiller, Thin Solid Films **446**, 37 (2004).
[15] R. M. Bradley and J. M. E. Harper, J. Vac. Sci. Technol. A **6**, 2390 (1988).
[16] C. Herring, J. Appl. Phys. **21**, 301 (1950).
[17] W. W. Mullins, J. Appl. Phys. **30**, 77 (1959).
[18] S. E. Orchard, Appl. Sci. Res. Sect. A **11**, 451 (1962).
[19] C. C. Umbach, R. L. Headrick, and K.-C. Chang, Phys. Rev. Lett. **87**, 246104 (2001).
[20] S. Vauth and S. G. Mayr, Phys. Rev. B **75**, 224107 (2007).
[21] J. F. Ziegler and J. P. Biersack, SRIM 2006.02 computer code, http://www.srim.org.
[22] *CRC Handbook of Chemistry and Physics* (CRC, Boca Raton, FL, 1984).
[23] S.-M. Wu, R. van de Kruijs, E. Zoethout, and F. Bijkerk, J. Appl. Phys. **106**, 054902 (2009).
[24] J. Bohdansky, Nucl. Instrum. Methods Phys. Res. B **2**, 587 (1984).
[25] E. Spiller, *Soft X-Ray Optics* (SPIE Optical Engineering, Bellingham, WA, 1994).